Invited talk at the Conference on Weak Interaction Physics, Bloomington, IN, May 16 - 17, 1977

LBL-6481

THE CASE FOR CHARMED MESON PRODUCTION IN e^+e^- ANNIHILATION AT SPEAR

Gerson Goldhaber

June 1977

Prepared for the U. S. Energy Research and Development Administration under Contract W-7405-ENG-48

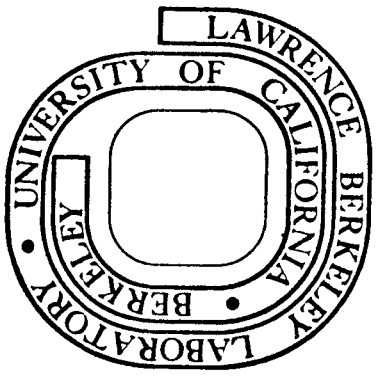

LBL-6481

DISCLAIMER

THE CASE FOR CHARMED MESON PRODUCTION IN e^+e^- ANNIHILATION AT SPEAR

Gerson Goldhaber
Department of Physics and Lawrence Berkeley Laboratory
University of California, Berkeley, California 94720

I. PRODUCTION AT SPEAR

The data I will discuss here comes from the SLAC-LBL magnetic detector at SPEAR. This detector as well as event selection techniques have been described earlier,[1] and I will thus confine myself to some details about the time-of-flight system only.

We have observed[2,3] a narrow resonance of mass 1865 MeV/c^2. In this talk I will present the evidence that this new particle -- and its associated excited state -- can be identified with the (D^o, D^+) and (D^{*o}, D^{*+}) doublets of charm theory.[4] Even though the evidence will develop in the course of this talk, I will use the accepted nomenclature for charmed particles from the outset.

The data sample analyzed here in the 3.9 - 4.6 GeV region corresponds to ~ 80,000 hadronic events identified in the detector. This data was taken in three roughly equal integrated luminosity runs, two at fixed energies E_{cm} = 4.028 and 4.415 GeV and one extending over an energy region from E_{cm} = 3.9 to 4.6 GeV. Furthermore we will also present more recent results from E_{cm} = 5.0 to 7.8 GeV. In the present analysis we have confined ourselves to hadronic events with three or more observed prongs.

Summary of Data Sample

E_{cm} (GeV)	Hadronic Events	Integrated Luminosity (pb^{-1})
3.9 - 4.6 pre-May 1976	29,000	1.8
4.028	25,000	1.3
4.415	26,000	1.6
5.0 - 7.8	160,000	17

The Particle Identification Methods by Time of Flight

Time-of-flight (TOF) information played an important part in this work. The TOF system includes 48 2.4 cm × 20 cm × 260 cm Pilot Y scintillation counters arranged in a cylindrical array immediately outside the tracking spark chambers at a radius of 1.5 m from the beam axis. Both ends of each counter are viewed by Amperex 56 DVP photomultiplier tubes (PM); anode signals from each PM are sent to separate TDC's, ADC's, and latches. Pulse height information is used to correct times given by the TDC's. The collision time is derived from a pickup electrode that senses the passage of the 0.2 ns long beam pulses; the period between successive collisions is 780 ns. Run-

to-run calibrations of the TOF system are performed with Bhabha scattering ($e^+e^- \rightarrow e^+e^-$) events. The rms resolution of the TOF system is $\sigma_t = 0.35 - 0.4$ ns.

Typical time difference between a π and a K in the Kπ signal is only about 0.5 ns. We have used the following two techniques to extract the best possible information on particle identity. To apply these methods, tracks are required to have good timing information from both PM's, consistent with the extrapolated position of the track in the counter.

A. Direct Particle Identification by TOF

In this method we calculate three χ_i^2 values for each observed track. They are related to the probability that the track is a π, a K, or a proton. Here χ_i^2 is defined by:

$$\chi_i^2 = (t_i - t_M)^2/\sigma_t^2$$

where $i = \pi, K, p$; t_i is the time calculated for mass i from measured momentum; t_M is measured TOF. If the track satisfies the criteria $\chi_K^2 < 3$, $\chi_K^2 < \chi_\pi^2$ the track is called a K; and similarly for protons. If $\chi_\pi^2 < \chi_K^2$ the track is called a π; the track is also called a π when no reliable TOF information is available as when, for example, more than one track hits the TOF counter.

B. The Weight Method

In the weight method each track is assigned three weights corresponding to its probability of being a π, K or p. These are determined from the measured momentum and TOF assuming a Gaussian probability distribution with standard deviation 0.4 ns. Then, the relative π-K-p probabilities are renormalized so that their sum is unity, and two-particle combinations are weighted by the joint probability that the particles satisfy the particular π or K hypothesis assigned to them. In this way, the total weight assigned to all $\pi\pi$, Kπ, and KK combinations equals the number of two-body combinations and no double-counting occurs.

To be more specific, we define

$$W_\pi \propto e^{-\chi_\pi^2/2}$$

$$W_K \propto e^{-\chi_K^2/2}$$

and $$W_p \propto e^{-\chi_p^2/2}$$

with the normalizing condition

$$W_\pi + W_K + W_p = 1 \quad .$$

In the study of the two-body meson system, for example, each pair of particles with total charge zero gets entered into three graphs:

in $M(\pi^{\pm}\pi^{\mp})$	we enter	$W_{\pi_1}W_{\pi_2}$
in $M(K^{\pm}\pi^{\mp})$	we enter	$W_{K_1}W_{\pi_2}$ and $W_{\pi_1}W_{K_2}$
in $M(K^{\pm}K^{\mp})$	we enter	$W_{K_1}W_{K_2}$.

In our earlier publications[2,3] we have used method B, the weight method. This method allowed us to give a quantitative assessment of the reliability of the K particle assignments in the D^o. In what follows we will use both method A, which lends itself more readily to the study of scatter plots, and method B. We will also show a comparison between the two methods which demonstrates that for the study of mass plots they do not differ in any essential features.

C. "Hidden" Charm

A glance at the distribution in $R = \sigma_{had}/\sigma_{\mu\mu}$ (see Figs. 1 and 2) shows clearly that some type of transition is occurring near E_{cm} = 3.8 GeV. Here we note the very narrow states $\psi/J(3095)$ and $\psi'(3684)$ are followed by a rapid step in R from an average value (excluding the ψ and ψ') of $\cong 2.5$ to an average value of $\cong 5$. In addition, evidence for several broader states (not fully resolved) around 4 GeV and one broad state at 4.415 GeV, Γ = 30 MeV is found.

Thus we see all the earmarks of narrow "bound" states* below 3.7 GeV, the ψ/J and ψ' with the quantum numbers of the photon. Furthermore, additional "bound" states with quantum numbers different from those of the photon, three to four** χ states,[5] reached by radiative decay from the ψ' and a state[6] $\chi(2800)$ reached by radiative decay of the ψ. Those are followed at higher E_{cm} values (above 3.8 GeV) by broad peaks, presumably no longer "bound" states.

The current interpretation is that these narrow particles are isosinglet states of a new quark-antiquark pair $c\bar{c}$, the charmonium states,[7] and that their decay is inhibited by the Okubo-Zweig-Iizuka (OZI) rule[8] where the final states do not contain the new quarks. This is similar to the case of the φ made up of $s\bar{s}$ whose decay to $\rho\pi$ is inhibited by the OZI rule as well.

The inhibition due to the OZI rule no longer applies as soon as the threshold energy is reached where the production of a pair of new mesons $D,\bar{D}$, each of which contain this new charmed quark c and $\bar{c}$ respectively, together with an old type quark ($\bar{q}_i$ and q_i respectively) becomes energetically allowed.

Experimentally one finds that the threshold for the new 1865 MeV/c^2 particles occurs right in the region between the narrow and broad peaks.

D. Charm "Revealed"

To show the evidence for charm I will discuss the following about the new particles:

*Here the term "bound" state is used to indicate that the decays are inhibited by a factor of $\sim$ 1000 over the normal strong interaction rates.

**$\chi(3415)$, $\chi(3500) \equiv P_c$, $\chi(3550)$ and possibly $\chi(3450)$.

a. The various neutral decay modes: $K^{\mp}\pi^{\pm}$, $K^{o}\pi^{+}\pi^{-}$, $K^{\mp}\pi^{\pm}\pi^{+}\pi^{-}$.
b. Observation of a threshold: $E_{th} > 3.1$ GeV and possibly > 3.7 GeV.
c. Exotic final state: the charged particle decays into an exotic final state $K^{\mp}\pi^{\pm}\pi^{\pm}$.
d. Associated production: the particles are produced exclusively in association with another particle of equal or larger mass.
e. Experimental width: from the direct mass measurement of the $K3\pi$ system we showed that the width is $\Gamma < 40$ MeV/c^2; by including information on the recoil system this can now be reduced to $\Gamma < 2$ MeV.
f. I-spin multiplets: the proximity in mass of the neutral and charged particles in both the ground state and first excited state is evidence that we are dealing with I-spin multiplets.
g. Radiative D^{*o} decay: from the recoil spectrum we show the presence of $D^{*o} \rightarrow \gamma D^{o}$. This is further evidence for the conservation of a new quantum number.
h. Parity violation in the decay: from a comparison of the $K\pi\pi$ and $K\pi$ decay modes we give evidence for parity violation, and hence weak decay.
i. Search for Cabibbo forbidden decay modes: we set an upper limit for decay in the $\pi^{+}\pi^{-}$ channel.
j. Semi-leptonic decay modes: evidence for these comes from work at DESY on inclusive e and $K^{o}e^{\pm}$ production cross sections.

II. THE ESTABLISHED DECAY MODES

A. Threshold Behavior for the $K^{\mp}\pi^{\pm}$ Decay Mode

In Fig. 3 we show the $K^{\mp}\pi^{\pm}$ mass distribution for three energy regions: the ψ/J, the ψ', and the $E_{cm} = 3.9 - 4.6$ GeV region as well as data at $E_{cm} = 4.028$ GeV. The D^{o} signal occurs only for the 3.9 - 4.6 GeV region. In particular we note that at $E_{cm} = 4.028$ GeV the signal-to-background ratio is considerably larger than for the overall 3.9 - 4.6 GeV region. The D is thus specifically associated with the resonance peaks in the total cross section. In Fig. 3 the ψ data corresponds to $\sim$ 150,000 hadronic events and the ψ' data to 350,000 hadronic events. We note that of these $\sim$ 72,000 hadronic events correspond to second-order electromagnetic interaction and these at least could in principle be a source for the D^{o} signal. We consider the absence of any such signal a clear indication that the D^{o} does not get produced below a threshold energy E_{th}. Thus $E_{th} > 3.1$ GeV, if we consider production via an intermediate photon. If we also consider direct production at the ψ', $E_{th} > 3.7$ GeV.

In Fig. 4 we show the $K\pi$ signal for all the $E_{cm} = 3.9 - 4.6$ GeV data with a cut on the recoil mass at $M_{recoil} > 1800$ MeV. This selection tends to reduce the background while the signal remains unaffected. Also shown in Fig. 4 are the kinematic reflections in the "$\pi^{+}\pi^{-}$" and "$K^{+}K^{-}$" mass distributions which occur because of K misidentification or lack of TOF information, in which case the track is assigned the pion mass. With the present statistics we note clear "kinematic reflection" signals at 1740 MeV/c^2 for "$\pi\pi$" and 1990 MeV/c^2 for "$K\bar{K}$." We note that the momentum of the two-body system in such a

kinematic reflection signal is not altered by the mass assignment to the track. We will make use of these additional events below in connection with the recoil spectrum.

The $K^{\mp}\pi^{\pm}$ signal is taken from the experimental mass distribution region $M(K\pi) = 1820 - 1900$ MeV/c^2. Background is estimated from two equal width side bands $M(K\pi) = 1700 - 1780$ MeV/c^2 and $M(K\pi) = 1940 - 2020$ MeV/c^2, a total of twice the width of the signal region. This gives a total signal after appropriate background subtraction ($\frac{1}{2} N_{bgnd}$) of 340 ± 47 events. The "$\pi^+\pi^-$" and "K^+K^-" reflection signals are obtained in a similar fashion and give signals of 159 ± 30 and 46 ± 11 events respectively. Thus if we ascribe all these three contributions to the D^o we get 545 ± 57 events.

B. The $(K3\pi)^o$ Decay Mode

In Fig. 5 we show the $K^{\mp}\pi^{\pm}\pi^+\pi^-$ mass distribution. Here the $D^o \to K3\pi$ signal suffers from a much more severe background problem than the $K^{\mp}\pi^{\pm}$ signal. The $K3\pi$ signal was determined for the mass interval 1860 - 1900 MeV/c^2 with two equal side bands for background determination. We find 325 ± 67 events in the signal after background subtraction.

C. The $K_S^o \pi^+\pi^-$ Decay Mode

Here we must first obtain a high quality K_S^o signal and then evaluate the $K_S^o\pi^+\pi^-$ mass combinations. Neutral kaons are identified by their decay $K_S \to \pi^+\pi^-$. In order to identify this decay and to suppress background from pions produced directly, the following procedure has been used. First, the event is projected onto the x-y plane, i.e., the plane perpendicular to the beams, and for any pair of oppositely charged particles the intersection of the tracks is determined. In order to assure good resolution on the vertex position the projected angle between the tracks is required to be at least 10^o and no more than 170^o. In general, one finds two intersections; the unphysical solution is usually far outside the detector and is eliminated by a cut on the distance from the beam. A minimum of 10 mm, corresponding to roughly four standard deviations away from zero, and a maximum of 16 cm, which is just inside the first wire chamber, is required. The vertex position obtained in projection is checked using the third coordinate. Tracks that are separated at the intersection by more than 16 cm with respect to z are rejected.

For the pairs selected in this way the total momentum is calculated as the vector sum of the momenta of the two tracks at the intersection. This vector is required to point back to the beam intersection. This is achieved by a four standard deviation cut on the angle between the momentum and the vector pointing from the beam to the vertex. This cut greatly enhances the signal-to-background ratio.[10] In Fig. 6 we show the resulting $K_S^o\pi^+\pi^-$ mass distribution for the $E_{cm} = 4.028$ GeV and 4.415 GeV data. A clear D^o signal is observed in each case corresponding to 62 and 50 events respectively.

D. The Charged Exotic Decay Mode $K^{\mp}\pi^{\pm}\pi^{\pm}(1876)$

In Fig. 7 we show a comparison of the exotic decay mode $K^{\mp}\pi^{\pm}\pi^{\pm}$ and the non-exotic mode $K^{\mp}\pi^{+}\pi^{-}$ for the "4.1" GeV region and with a cut on the recoil system: $M_{rec} = 1960 - 2040$ MeV/c^2.

Here "exotic" stands for the fact that the I-spin of the final state is $I = 3/2$ or $5/2$ rather than $I = 1/2$ as is the case for all known K^*'s. Such a final state cannot be formed out of a $q_i\bar{q}_j$ pair where here q_i ($\bar{q}_j$) stands for any of the three "old-fashioned" quarks (anti-quarks). Another way of describing the "exotic" nature of this final state is that the charge of the K is opposite to the charge of the entire $K\pi\pi$ final state. In terms of the charm model[4] the Cabibbo-favored decays involve a c-quark transforming into an s-quark with $\Delta C = \Delta S$. Thus the D^+ with $C = 1$ and $S = 0$ decays to a system with $C = 0$, $S = -1$ and positive charge, which is exotic. The exotic $K\pi\pi$ signal was determined from the mass interval 1840 - 1920 MeV/c^2. Here background estimates come from the non-exotic channel over the same mass interval, scaled by 1/2. We find 75 ± 12 events in the signal after background subtraction, and 160 ± 35 events in the entire data sample.

III. THE RECOIL SYSTEMS, PRODUCTION AND DECAY MODES

We find that the D^o and D^+ signals are associated with very distinct recoil spectra. Here M_{recoil} is defined by:

$$M^2_{recoil} = (E_{cm} - \sqrt{p^2 + M^2})^2 - p^2$$

where M and p are the measured effective mass and momentum of the final state considered. Alternately if we consider M as a δ-function, we can substitute a nominal fixed value of $M(D^o) = 1865$ MeV and $M(D^+) = 1872$ MeV for M respectively.

In Fig. 8a we show the M_{recoil} distribution as measured directly and in Fig. 8b with $M_{K\pi}$ fixed for all the data. In Fig. 8a only the $K\pi$ signal with identified K mesons is shown. On the other hand in Fig. 8b we have also added in the signal from the "$\pi^+\pi^-$" and "K^+K^-" kinematical reflections illustrated in Fig. 4. This is possible as only the experimental quantities E_{cm} and the momentum p are used to calculate M_{recoil}. The addition of these signals increases the available statistics, but more important, removes biases due to the fact that the reliability of K identification decreases with increasing K momentum. In view of the fact that the D momentum p is essentially unaffected by the constituent particle identities, this procedure becomes independent of the TOF mass assignments (except for nucleon elimination). The only small mass dependent contribution to particle momenta comes from the energy loss in the beam pipe and its surrounding trigger counters ~ 1.9 gm/cm^2 of material. In the distributions in Figs. 8a and 8b the corresponding background has been subtracted. The background was evaluated from the population of two bands on either side of the signal. In Fig. 8a the background bands were subtracted directly without concern for slightly different kinematical boundaries. In Fig. 8b M_{recoil} for the background events was evaluated with the

same fixed $M_{K\pi}$ value. This "scales" the kinematic boundaries.

Some caution must be used in interpreting the four prominent structures in Fig. 8b. Namely, we must remember that the data samples added together in this figure have a highly non-uniform integrated luminosity distribution from $E_{cm} = 3.9 - 4.6$ GeV. In particular the second and third peaks come largely from the 4.028 GeV data. We observe narrow peaks in M_{recoil} at $\cong 1860$ MeV/c^2, $\cong 2005$ MeV/c^2, $\cong 2145$ MeV/c^2 and a broader peak at $\cong 2440$ MeV/c^2. We interpret the first three peaks as follows[10]:

$$e^+e^- \rightarrow D^oD^o \quad (1)$$

$$e^+e^- \rightarrow D^o\bar{D}^{*o} \text{ and } \bar{D}^oD^{*o} \quad (2)$$

$$e^+e^- \rightarrow D^{*o}\bar{D}^{*o} \ . \quad (3)$$

A priori, an alternate possibility exists for the third peak; viz.,

$$e^+e^- \rightarrow D^oD^{**o} \text{ and charge conjugate} \ . \quad (3')$$

We will discuss these interpretations in more detail below and in particular show evidence to rule out interpretation (3'). The enhancement at 2440 MeV/c^2 and width $\Gamma \cong 100$ MeV/c^2 could be due to multibody processes such as $D^*\bar{D}^*\pi$, for example or, alternatively, production of a charmed state of higher mass.

The recoil spectrum against the $(K3\pi)^o$ mass peak shows consistent features (Fig. 8c) but suffers statistically from the very substantial background subtraction.

In Fig. 9 we show the corresponding M_{recoil} distribution for the exotic channel $K^\mp\pi^\pm\pi^\pm$. In this case the background is deduced from the non-exotic channel $K^\pm\pi^+\pi^-$. Here we again have a more severe background subtraction as well as a lower statistical significance on the signal (~ 160 events). The very prominent peak observed at $M_{recoil} \sim 2010$ MeV/c^2 can be interpreted as

$$e^+e^- \rightarrow D^+D^{*-} \text{ and charge conjugate} \ . \quad (4)$$

There are indications in the data for the presence of the other three peaks observed in the recoil spectrum against the D^o. In particular there is evidence for

$$e^+e^- \rightarrow D^{*+}D^{*-} \ , \quad (5)$$

only weaker relative to reaction (4).

A. D^* Decay Modes

The possible charm conserving D^* decay modes are:

$D^{*o} \rightarrow \gamma D^o$	observed	(6)
$D^{*o} \rightarrow \pi^o D^o$	observed	(7)
$D^{*o} \rightarrow \pi^- D^+$	kinematically forbidden	(8)
$D^{*+} \rightarrow \gamma D^+$	one or both observed	(9)
$D^{*+} \rightarrow \pi^o D^+$	one or both observed	(10)
$D^{*+} \rightarrow \pi^+ D^o$	observed	(11)

The evidence for the observed decay modes is given below. It is interesting to note that if charm were violated, D^*'s would preferentially decay strongly into light hadrons rather than electromagnetically.

B. $D^*\bar{D}^*$ Production

The evidence for reaction (3) is given in Figs. 10 and 11. Figure 10a shows combined $K\pi$, $K3\pi$ subtracted recoil spectra taken at $E_{cm} = 4.028$ GeV. The spectrum is dominated by two narrow peaks at masses near 2005 and 2145 MeV/c^2. There is weaker evidence for a peak at 1860 MeV/c^2 corresponding to $D^0\bar{D}^0$ production. A similar spectrum for events taken in the range $4.35 < E_{cm} < 4.5$ is presented in Fig. 10b. Again there is a peak near the recoil mass 2005 MeV/c^2, however the higher mass peak has moved to 2200 MeV/c^2 and has broadened. The 2005 MeV/c^2 peak we interpret as the state D^{*0}. The peak near 2145 MeV/c^2 moves with E_{cm} in the manner expected for a kinematic reflection arising from D^* pair production followed by a π^0 decay of one D^* to the observed D^0. The same data are shown in Fig. 11 for the $K\pi$ recoil spectrum only. Superimposed on Fig. 11 are the expected shapes for these two peaks at the two respective E_{cm} values computed with nominal masses of $M_D = 1865$ and $M_{D^*} = 2005$ MeV/c^2. In computing the reflection peak, we have assumed that the D^* cascades into the D via pion emission (decay mode (7)). Thus the results of Figs. 10 and 11 can be interpreted as D^0 production through the reactions (1) - (3). These production processes are discussed by De Rujula, Georgi, and Glashow, and Lane and Eichten[11] based on our early preliminary results.

IV. THE DECAY MODE $D^{*+} \rightarrow \pi^+ D^0$

There are two features which contribute to the fact that the decay mode $D^{*+} \rightarrow \pi^+ D^0$ cannot be directly observed in the 3.9 - 4.6 GeV region.

(i) The Q value for decay mode (11) is small, hence the π^+ and D^0 have momenta roughly proportional to their masses.

(ii) At low momenta (< 100 MeV/c) our detector becomes very inefficient for charged particle detection. It cuts off completely below $p_\perp = 55$ MeV/c where $p_\perp$ is the momentum projection perpendicular to the beam axis.

We have thus examined the $E_{cm} = 5.0 - 7.8$ GeV region where for high D^{*+} momenta the decay π^+ becomes readily detected.[12] In Fig. 12 we show the $K^\mp\pi^\pm$ mass distribution for D^0 momenta > 1.5 GeV/c. Here we use the TOF method B. We note a clear although somewhat broader D^0 peak. We then select $K\pi$ combinations in the D^0 signal (1820 - 1910 MeV/c^2) and compute the $D^0\pi^\pm$ mass combinations. The quantity that is precisely measured is the mass difference $M(D^0\pi) - M(D^0)$. This mass difference is plotted in Fig. 13. From this data we find the $D^{*+} - D^0$ mass difference to be 145.3 ± 0.5 MeV/c^2 or equivalently the Q value for decay mode (11) is 5.7 ± 0.5 MeV. We will use this information as a constraint in the mass determinations below. The observed width of the peak in Fig. 13a is consistent with the expected resolution from Monte-Carlo calculations. Thus $\Gamma(D^{*+}) < 2$ MeV/c^2. This implies that even though we are dealing with a strong charm conserving decay, be-

cause of the small Q value for p wave pion decay Γ is rather small. This same limit also holds for the D^o; viz., $\Gamma(D^o) < 2$ MeV/c^2. Here of course we expect the true Γ to be $\ll 1$ eV.

V. MASSES AND RELATIVE PRODUCTION RATES

For mass determination we focus on a single energy: $E_{cm} = 4.028$ GeV. We can then consider momentum distributions p of the two-particle system. In Fig. 12b we show the momentum spectrum for the two-body decays of the D^o, in 10 MeV intervals. In Fig. 12c the same for the $K^{\mp}\pi^{\pm}\pi^{\pm}$ system. Figure 12a illustrates the various processes contributing to the D^o spectrum.

A. Central Momentum Values

Several peaks stand out prominently:

$$p_1 = 765 \pm 12 \text{ MeV/c} ,$$
$$p_2 = 560 \pm 8 \text{ MeV/c} ,$$
$$p_3 = 178 \pm 8 \text{ MeV/c} ,$$

for the neutral distributions and

$$p_4 = 535 \pm 10 \text{ MeV/c}$$

for the charged distribution. Here the indices correspond to the reactions quoted above. The errors are estimates of the precision to which the central values are known including an allowance for systematic errors in the momentum scale. Finally the incident energy is

$$E_{cm}/2 = E_o = 2014 \pm 2.7 \text{ MeV} .$$

Here the error has three components added in quadrature: $\pm$ 2 MeV from the 0.1% uncertainty in the absolute energy calibration, $\pm$ 1.4 MeV beam spread from synchrotron radiation effects, and $\pm$ 1 MeV variation (which is known from flip coil measurements) in precise run-to-run beam settings. The absolute energy calibration is tied to the ψ mass value of 3095 MeV/c^2. We do not include this scale uncertainty in the mass errors quoted below. As far as widths of distributions are concerned the latter two errors contribute in quadrature giving dE_o = 1.7 MeV.

B. Momentum Spectra

From a glance at Fig. 14a we note three distinct contributions to the peak corresponding to $D^{*-}\bar{D}^{*}$ production, process (3), depending on the source of the observed D^o's. It is clear that the shape of the peak centered at p_3 is a sensitive function of whether we are dealing with π^o or γ decay of D^{*o}. For π^o decay we get a Gaussian distribution while for γ decay we get a distribution with dN/dp^2 = constant or $dN/dp \propto p$, which results in a triangular shape. Finally for D^o production from the D^{*+} feeddown decay mode, process (11), we expect a separate peak. As there is no evidence for such a peak this means that either the D^{*o} and D^{*+} masses are nearly degenerate, or the rate

of contributions from process (11) is low. The value of the D^* mass, for process (7) or (11), is a sensitive function of p_3; viz., $dM(D^*) \cong -0.1\, dp_3$.

The second peak and its associated shoulder is due to $D\bar{D}^*$ (and charge conjugate) production, process (2). Here as we note from Fig. 14a there are four contributing processes. The central value of p_2 determines $M_D + M_{D^*}$, while the shape of the shoulder and peak determine the relative contributions of the four processes. Finally the third "peak" (which appears clearly in a 20 MeV/c binning) is due to $D\bar{D}$ production, process (1). A similar -- though simpler -- situation holds for the D^+ spectrum.

When high statistical accuracy becomes available it should be possible to determine all masses and production cross sections as well as the $B(D^+ \to K^-\pi^+\pi^+)/B(D^o \to K^-\pi^+)$ ratio of branching ratios from two such spectra. In view of the present limited statistics, particularly in the D^+ spectrum, we have carried two types of fits to the data in Fig. 14.

Type I - Normal fit

Here we make the assumptions:

(a) All D and D^* production occurs through two-body reactions, processes (1 - 3) and their charged analogue.

(b) All allowed D^* decay processes are given by (6 - 11) (except for (8)).

(c) D^* decays are isotropic in the D^* rest frame.

Assumption (a) was tested by including in the assumed D^o spectrum the three-body process $D^o\bar{D}^o\pi^o$. This process produces a very broad peak centered near 400 MeV/c that is not seen in the data. We estimate that it contributes less than 10% of the D^o signal. Decay mode (11) complicates the momentum spectra because it couples produced D^{*+} events to observed D^o events.

D^o and $D^\pm$ momentum spectra expected under these assumptions, folded with detector resolution, were simultaneously fit to the data by varying the parameters shown in the first column of Table I. The Q-value for decay mode (11) was fixed at 5.7 MeV as stated above. The momentum spectrum for background events was estimated by smoothing the spectrum of the background events discussed above.

Type II - Isospin constrained fit

A second fit to the data was performed with the additional assumptions:

(d) D and D^* are produced at $E_{cm} = 4.028$ GeV in states of pure isospin and the phase space corrections to reactions (1), (2) and (3) follow a p^3 law, where p is the center-of-mass momentum.

(e) Isospin is a good quantum number in pionic decays of D^*, and the transition probability decay mode (9) is 1/4 that of decay mode (6).[13] Phase space corrections for D^* decay also behave like p^3, where p is now the momentum of the D in the D^* rest frame.

The p^3 dependence follows from the assumption[14] that the D and D^* are pseudoscalar and vector respectively. The data were fit under both sets of assumptions with various starting points, background functions, and resolutions in order to study the stability of the results. Some parameters vary outside of statistical errors depending on the type of fit.

To get a feeling for these two types of fits in columns 2 and 3 of Table I we show average values obtained from a number of different versions of these fits, while in column 4 of the Table, we present the parameters we judge to be most reliably determined along with our estimate of their total uncertainty including systematic errors. The solid curves of Figs. 14b and 14c show the results of a typical fit of the second type. It is important to note that the population at low momenta in Fig. 14c is too large to be interpreted as just background. Indeed if one restricts the $K\pi\pi$ invariant mass analysis to combinations having momentum less than 320 MeV/c, one finds a three standard deviation peak at the D^+ mass. The natural interpretation of this result is the presence of significant $D^{*+}D^{*-}$ production followed by decays via modes (9) and/or (10).

We note from Table I that the extent of the D^o contribution due to decay mode (11) is highly model dependent. In fits of the first kind, only 6% of observed D^o's can be attributed to D^{*+} production followed by decay mode (11). In the isospin constrained fits, this fraction increases to 29%. Because of this large value the isospin constrained fit forces the D^{*o} and D^{*+} masses to be nearly equal in order to match the narrowness of the peak near 180 MeV/c in Fig. 14b.

We note from Table I that the relative importance of reactions (1), (2), (3) for the D^o, D^{*o} channels can be expressed as:

$$D^o\bar{D}^o \ : \ D^o\bar{D}^{*o} + \bar{D}^oD^{*o} \ : \ D^{*o}\bar{D}^{*o}$$

$$0.2 \pm 0.1 \ : \quad 4.0 \pm 0.8 \quad : \ 128 \pm 40$$

where a p^3 phase space factor has been explicitly removed. These ratios are to be compared with the spin counting estimates[11] of 1:4:7, which are in strong disagreement with the data. Various explanations of this behavior have been discussed in the literature.[11,15]

Furthermore we note that $M_{D^+} > M_{D^o}$. This mass difference has been predicted in the literature.[11,16,17] More measurements will be needed to establish an actual reliable value for this mass difference.

VI. THE τ-θ PUZZLE REVISITED; EVIDENCE FOR PARITY VIOLATION FROM D DECAY

A study of the $D^\pm \to K\pi\pi$ Dalitz plot shows that the plot is compatible with a phase space distribution, does not appear to die off on the boundaries as a natural spin parity assignment would, and is specifically incompatible with J^P assignments of 1^- or 2^+. These observations, coupled with the observation of the $K\pi$ decay of the D^o, a final state of natural spin parity ($J^P = 0^+, 1^-, 2^+, \ldots$), and the belief that the neutral and charged particles are members of the same isomultiplet, suggest parity violation in the decay of the D's.

A. Appearance of Dalitz Plot

In order to obtain a relatively clean sample of the decay $D^\pm \to K^\mp\pi^\pm\pi^\pm$ we apply mass and missing mass cuts to three-body combinations for data taken between $3.9 < E_{cm} < 4.25$ GeV. The cuts are $1860 < M_{K\pi} < 1920$ MeV/c^2 and $1960 < M_{recoil} < 2040$ MeV/c^2 (see Fig. 7). From this selection we obtain a sample of 126 events of which we esti-

mate 58 events to be background. In Fig. 15a we present the Dalitz plot for these 126 events, choosing the Dalitz variables:

$$X_{\text{Dalitz}} = \frac{\left|T_{\pi_1} - T_{\pi_2}\right|}{\sqrt{3}\,Q} \; ; \; Y_{\text{Dalitz}} = \frac{T_K}{Q}$$

with T being D rest frame kinetic energies and $Q = T_{\pi_1} + T_{\pi_2} + T_K$. Figure 15b shows a background Dalitz plot consisting of non-exotic $K\pi\pi$ combinations, $K^{\pm}\pi^{+}\pi^{-}$, with identical kinematic cuts. Both the signal and background plots appear uniformly populated without either boundary zeros or zeros along the y axis as expected for natural spin parity assignment. In order to specifically rule out the states 1^- and 2^+ we have performed Monte-Carlo simulations using the simple, phenomenological matrix elements presented by Zemach.[18]

B. The 1^- Matrix Element

For the case of $J^P = 1^-$ we construct an axial vector amplitude symmetric under the exchange of the two pions. A simple representation is provided by: $(T_{\pi_1} - T_{\pi_2})(\vec{\pi}_1 \times \vec{\pi}_2)$ where $\vec{\pi}$ represents a D rest frame pion momentum. For the case of unpolarized production one then expects an intensity

$$I_{1^-} \propto \left|T_{\pi_1} - T_{\pi_2}\right|^2 \left|\vec{\pi}_1 \times \vec{\pi}_2\right|^2 \quad .$$

To compare the distribution of I_{1^-} with the data, we have divided the Dalitz plot into two discrimination regions divided by a contour of constant I_{1^-}. The particular contour was chosen so that an equal number of events would be found in each region for a phase-space decay of the state D^+, as determined by a Monte-Carlo calculation. Because of the approximately uniform $K\pi\pi$ detection efficiency over the Dalitz plot these regions have nearly equal areas. Figures 13c and 13d show the $K^{\mp}\pi^{\pm}\pi^{\pm}$ invariant-mass spectra for events with Dalitz variables lying inside the two 1^- discrimination regions as indicated by the shaded area in the respective insets.

A fit to a Gaussian signal over the scaled background of Fig. 7b reveals 34 ± 9 signal events in the peripheral region compared to 38 ± 9 signal events in the central region. Such a division is consistent with equal population with a χ^2 of 0.1 for one degree of freedom (DF) or a confidence level CL = 75%. On the other hand, a Monte-Carlo simulation of $K\pi\pi$ decays using the intensity distribution I_{1^-} gives an expected population division of 1:8.2 for peripheral to central region. This is effectively ruled out with a χ^2 of 18.1 ($CL = 2 \times 10^{-5}$).

C. The 2^+ Matrix Element

Again following Zemach[18] we construct a symmetric, traceless second-rank tensor which is also symmetric under the exchange of the two pions. A simple example is provided by: $A^{ij} = \Delta\pi^i q^j + \Delta\pi^j q^i$ where $\overrightarrow{\Delta\pi}$ is the difference of the pion momenta and $\vec{q}$ is their cross product.

For unpolarized production one expects intensity proportional to

$$\sum_i \sum_j A^{ij} A_{ji} \quad \text{or} \quad I_{2^+} \propto |\vec{\pi}_1 - \vec{\pi}_2|^2 |\vec{\pi}_1 \times \vec{\pi}_2|^2 \ .$$

Similarly we find that I_{2^+} depopulates the peripheral region relative to the central region by 1:5.6 (see Figs. 16b and 16c). Our fits give 31 ± 9 events in the peripheral regions and 35 ± 10 events in the central region. This result is again consistent with equal population with a χ^2 of 0.1 for one DF (CL = 75%), and inconsistent with I_{2^+} with a χ^2 of 9.4 for one DF (CL = 0.002). The observed sample population of the 2^+ peripheral discrimination region indicates the absence of a general boundary zero. The absence of such a zero argues against natural spin and parity final states of spin 3 and greater as well.

We have thus demonstrated from a study of the $K\pi\pi$ Dalitz plot that this three-body final state is incompatible with J^P assignments of either 1^- or 2^+ as well as higher natural spin parity values. $J^P = 0^+$ is not an allowed state of three pseudoscalars. Since the presumed isomultiplet state, D^0, decays into two pseudoscalars, a final state of natural spin parity, we conclude there exists evidence for parity violation in the decays of the D's, which implies that we are dealing with a weak decay.

VII. SEARCH FOR A CABIBBO FORBIDDEN DECAY MODE

According to charm theory[4] the decay $D^0 \to K^-\pi^+$ proceeds with a BR $\propto \cos^2\theta$ while the decay $D^0 \to \pi^-\pi^+$ proceeds with a BR $\propto \sin^2\theta$ where θ is the Cabibbo angle. We have searched for a $\pi^-\pi^+$ signal with optimal cuts on the recoil system. We can set an upper limit of $BR(D^0 \to \pi^+\pi^-)/BR(D^0 \to K^-\pi^+) < 0.07$ at the 90% CL.

VIII. $D^0 - \bar{D}^0$ MIXING

We have obtained two independent results related to the question of $D^0 - \bar{D}^0$ mixing.[19]

A. Test for Strangeness Conservation

In the $E_{cm} = 3.9 - 4.6$ GeV data we have established an upper limit on charm events exhibiting apparent strangeness violation; i.e., events where the kaon observed in the recoil system has the same charge as the kaon found in the D^0. This study bears on the question of $D^0 - \bar{D}^0$ mixing. Using the TOF kaon identification technique, method A, we find 77 events in our total data sample with a D^0(or $\bar{D}^0$) $\to K^{\mp}\pi^{\pm}$ candidate and an additional kaon in the recoil system. We estimate that 39% of these events correspond to background.* In the signal region the two kaons have like charge in 15 events and thus a like charge fraction of 20 ± 5%, while for the background regions we obtain 32 ± 6% for this fraction. After background corrections we find a like charge fraction of 12 ± 9%. This fraction is consistent with 13%, the fraction obtained by a Monte-Carlo simulation predicated on no $D^0 - \bar{D}^0$ mixing, thus suggesting that the 12% apparent strangeness violation is primarily due to residual time-of-flight misidentification. After correcting for this effect, we find that less than 18% of events containing a D^0 exhibit an apparent strangeness violation (90% CL).

*We have applied recoil mass cuts to the data in order to achieve this low background level.

It has been suggested[20] that the presence of first-order $|\Delta C| = 2$ neutral currents would create $D^0 - \bar{D}^0$ mixing on time scales considerably shorter than the D^0 lifetime. If this were true, nearly 1/2 of events containing a D^0 would exhibit strangeness nonconservation. Our results clearly rule this out.

B. Test for D^{*+} Exotic Decay

In the $E_{cm} = 5 - 7.8$ GeV data we have tested whether the decay proceeds as:

$$D^{*+} \rightarrow \pi^+ D^0 \quad \big|\rightarrow K^-\pi^+ \qquad \text{(exotic final state)}$$

as expected for no $D^0 - \bar{D}^0$ mixing, or as:

$$D^{*+} \rightarrow \pi^+ \bar{D}^0 \quad \big|\rightarrow K^+\pi^- \qquad \text{(nonexotic final state)}$$

which would imply such mixing. To this end we study the possible $D^0\pi^-$ signal near a mass difference of 145 MeV/c^2 in Figs. 13b and 13d. These events could be caused by three effects: (1) double misidentification of a π as a K and a K as a π, (2) $\Delta C = -\Delta S$ decays, which are expected to be suppressed by $\tan^4\theta_C$ ($\sim 2 \times 10^{-3}$), or (3) $D^0 - \bar{D}^0$ mixing. To eliminate the first possibility as much as possible, we select the events from Figs. 13c and 13d within 2.5 MeV/c^2 of the center of the peak and require that the ratio of the time-of-flight weights for the chosen combination to that for the combination in which the K and π have been interchanged be greater than 3.[21] Out of 38 $D^0\pi^+$ events 26 survive and out of 11 $D^0\pi^-$ events 3 survive. These latter 3 events are consistent with coming from backgrounds. We expect 1.4 events from uncorrelated combinations of particles and 0.6 events from $K\pi$ double misidentification. Thus, at the 90% confidence level, the fraction of the time that a D^0 decays as if it were a $\bar{D}^0$ (e.g., to $K^+\pi^-$ instead of $K^-\pi^+$) is less than 16%. The relationship between these two measurements depends in detail on the D^0 production mechanism over the full energy range from 3.9 to 4.6 GeV, which is unknown at present. A discussion of this relationship appears in R. L. Kingsley.[19]

The results presented here are the work of the LBL-SLAC collaboration at SPEAR, whose members are: G. S. Abrams, M. S. Alam, A. M. Boyarski, M. Breidenbach, W. C. Carithers, W. Chinowsky, S. Cooper, J. M. Dorfan, G. J. Feldman, D. Fryberger, G. Hanson, J. Jaros, A. D. Johnson, J. A. Kadyk, R. R. Larsen, D. Lüke, V. Lüth, H. L. Lynch, R. J. Madaras, H. K. Nguyen, J. M. Paterson, M. L. Perl, I. Peruzzi, M. Piccolo, F. M. Pierre, T. P. Pun, P. Rapidis, B. Richter, R. H. Schindler, R. F. Schwitters, J. Siegrist, W. Tanenbaum, G. H. Trilling, and J. E. Wiss.

We wish to thank the LBL and SLAC computer centers for their help in facilitating the data analysis. Finally I wish to thank Ms. Christina Frank for her meticulous work in typing and compiling this report.

This work was supported by the U. S. Energy Research and Development Administration.

REFERENCES AND FOOTNOTES

1. J.-E. Augustin et al., Phys. Rev. Lett. 34, 233 (1975); J.-E. Augustin et al., Phys. Rev. Lett. 34, 764 (1975).
2. G. Goldhaber et al., Phys. Rev. Lett. 37, 255 (1976).
3. I. Peruzzi et al., Phys. Rev. Lett. 37, 569 (1976).
4. S. L. Glashow, J. Iliopoulos, and L. Maiani, Phys. Rev. D2, 1285 (1970); S. L. Glashow, Experimental Meson Spectroscopy, A.I.P. Conf. Proc. No. 21, Particles and Fields Subseries No. 8, p. 387 (1974). For more details, see also M. K. Gaillard, B. W. Lee, and J. L. Rosner, Rev. Mod. Phys. 47, 277 (1975); A. De Rujula, H. Georgi, and S. L. Glashow, Phys. Rev. D12, 147 (1975); M. B. Einhorn and C. Quigg, Phys. Rev. D12, 2015 (1975). Earlier indications of possible charmed particle production have come from experiments involving neutrino interactions, as well as from cosmic-ray emulsion studies. See, for example: A Benvenuti et al., Phys. Rev. Lett. 34, 419 (1975); E. G. Cazzoli et al., Phys. Rev. Lett. 34, 1125 (1975); J. Blietschau et al., Phys. Lett. 60B, 207 (1976); J. von Krogh et al., Phys. Rev. Lett. 36, 710 (1976); B. C. Barish et al., Phys. Rev. Lett. 36, 939 (1976); K. Niu et al., Prog. Theor. Phys. 46, 1644 (1971). Subsequent to our work, evidence for a charmed baryon has also been presented from a photoproduction experiment at the Fermilab; B. Knapp et al., Phys. Rev. Lett. 37, 882 (1976).
5. W. Braunschweig et al., Phys. Lett. 57B, 407 (1975); W. Tanenbaum et al., Phys. Rev. Lett. 35, 1323 (1975); G. J. Feldman et al., Phys. Rev. Lett. 35, 821 (1975). For a more recent review, see G. H. Trilling, Study of Intermediate States Produced by Radiative Decays of ψ, talk presented at the Summer Institute on Particle Physics, SLAC, August 1976, LBL-5535.
6. See, for example, B. H. Wiik, XVIIIth International Conference on High-Energy Physics, Tbilisi, USSR, July 1976.
7. T. Appelquist et al., Phys. Rev. Lett. 34, 365 (1975); E. Eichten et al., Phys. Rev. Lett. 34, 369 (1975).
8. S. Okubo, Phys. Lett. 5, 105 (1963); G. Zweig, CERN Report Th-401, 412 (1964), unpublished; J. Iizuka, K. Okada and O. Shito, Prog. Theor. Phys. 35, 1061 (1966).
9. J. Burmester, Phys. Lett. 64B, 369 (1976).
10. V. Lüth et al., Phys. Lett. (in press, 1977).
11. A. De Rujula, H. Georgi, and S. L. Glashow, Phys. Rev. Lett. 37, 398 (1976); K. Lane and E. Eichten, Phys. Rev. Lett. 37, 477 (1976).
12. G. J. Feldman et al., Phys. Rev. Lett. 38, 1313 (1977).
13. S. Ono, Phys. Rev. Lett. 37, 655 (1976).
14. H. K. Nguyen et al., LBL-6424 and SLAC-PUB-1946; J. E. Wiss et al., Phys. Rev. Lett. 37, 1531 (1976).
15. A. De Rujula, H. Georgi, and S. L. Glashow, Phys. Rev. Lett. 38, 317 (1977); M. Suzuki, Phys. Rev. Lett. 37, 1164 (1976); D. McKay and B. Young, Phys. Rev. D15, 1282 (1977).
16. D. B. Lichtenberg, Phys. Rev. D12, 3760 (1975).
17. K. Lane and S. Weinberg, Phys. Rev. Lett. 37, 717 (1976); H. Fritzsch, Phys. Lett. 63B, 419 (1976); Lai-Him Chan, Phys. Rev. D15, 2478 (1977).

18. C. Zemach, Phys. Rev. B133, 1201 (1964). See also B. Lee, C. Quigg, and J. L. Rosner, Comments on Nuclear and Particle Physics VIIA, 49 (1977).
19. M. K. Gaillard, B. W. Lee, and J. L. Rosner, Rev. Mod. Phys. 47, 277 (1975); R. L. Kingsley, S. B. Treiman, F. Wilczek, and A. Zee, Phys. Rev. D11, 1919 (1975); L. B. Okun, V. I. Zakharov, and B. M. Pontecorvo, Lett. Nuovo Cimento 13, 218 (1975); A. De Rujula, H. Georgi, and S. L. Glashow, Phys. Rev. Lett. 35, 69 (1975); A. Pais and S. B. Treiman, Phys. Rev. D12, 2744 (1975); R. L. Kingsley, F. Wilczek, and A. Zee, Phys. Lett. 61B, 295 (1976); K. Kang and J. E. Kim, Phys. Lett. 64B, 93 (1976); R. L. Kingsley, Phys. Lett. 63B, 329 (1976); M. Goldhaber and J. L. Rosner, Phys. Rev. D15, 1254 (1977).
20. See for example, S. L. Glashow and S. Weinberg, Phys. Rev. D15, 1958 (1977) and E. A. Paschos, Phys. Rev. D15, 1966 (1977).
21. It should be noted that our $D^0 - \bar{D}^0$ discrimination comes from both the TOF information and the requirement used in constructing Fig. 13 that the observed $K\pi$ mass lie in the range 1820 to 1910 MeV/c^2.

Table I. Results from simultaneous fits to the D^o, D^+ momentum spectra at E_{cm} = 4.028 GeV.

	Fit parameter	Normal fit	Isospin constrained fit	Estimated values
Masses in MeV/c^2	M_{D^o}	1864 (1.5)[a]	1862 (0.5)[a]	1863 ± 3[b]
	M_{D^+}	1874 (2.5)	1873 (2.0)	1874 ± 5
	$M_{D^{*o}}$	2006 (0.5)	2007 (0.5)	2006 ± 1.5
	$M_{D^{*+}}$	2009 (1.5)	2007 (0.5)	2008 ± 3
Branching ratios	$BR(D^{*o} \to \gamma D^o)$	0.45 (0.08)	0.75 (0.05)	0.55 ± 0.15
	$BR(D^{*+} \to \pi^+ D^o)$[c]	--	0.60 ± 0.15	--
	$\frac{BR(D^+ \to K^- \pi^+ \pi^+)}{BR(D^o \to K^- \pi^+)}$[c]	--	1.60 ± 0.60	--
D^o source fractions	$D^o\bar{D}^o$	0.05 (0.03)	0.05 (0.02)	0.05 ± 0.03
	$D^o\bar{D}^{*o} + \bar{D}^o D^{*o}$	0.42 (0.04)	0.34 (0.04)	0.38 ± 0.08
	$D^{*o}\bar{D}^{*o}$	0.47 (0.05)	0.32 (0.05)	0.40 ± 0.10
	$D^{*+}D^-$; $D^{*+} \to \pi^+ D^o$	0.03 (0.02)	0.09 (0.04)	0.06 ± 0.05
	$D^{*+}D^{*-}$; $D^{*+} \to \pi^+ D^o$	0.03 (0.03)	0.20 (0.07)	0.11 ± 0.10
D^+ source fractions	D^+D^-	0.09 (0.05)	0.09 (0.05)	0.09 ± 0.05
	$D^{*+}D^- + D^{*-}D^+$	0.65 (0.07)	0.58 (0.06)	0.62 ± 0.09
	$D^{*+}D^{*-}$	0.26 (0.08)	0.33 (0.08)	0.29 ± 0.10

[a] Quantities in parentheses are statistical errors from the fitting process.

[b] Errors quoted include estimated systematic uncertainty.

[c] These values can only be obtained under the assumptions of the isospin constrained fit. The quoted errors do not reflect possible breakdown of these assumptions.

FIGURE CAPTIONS

Fig. 1. The ratio $R = \sigma_{had}/\sigma_{\mu\mu}$. The ψ/J and ψ' including their radiative tails have been subtracted out.

Fig. 2. Details of the ratio $R = \sigma_{had}/\sigma_{\mu\mu}$ in the 3.9 - 4.6 GeV region. The distribution corresponds to the pre-May 1976 data sample. The location of the two high-statistics points 4.028 and 4.415 GeV is also indicated.

Fig. 3. A composite of the $K\pi$ mass distribution for the ψ/J region, the ψ' region and the $E_{cm} = 3.9 - 4.6$ GeV region (all data) as well as the $E_{cm} = 4.028$ GeV data separately.

Fig. 4. The two-body mass distributions with $M_{recoil} > 1800$ MeV/c for all data. (a) $K^{\mp}\pi^{\pm}$, (b) "$\pi^+\pi^-$," (c) "K^+K^-" and insert (d) which shows the $K^{\mp}\pi^{\pm}$ distributions as obtained by the two TOF methods for the $E_{cm} = 4.028$ GeV data only.

Fig. 5. The $K^{\mp}\pi^{\pm}\pi^+\pi^-$ mass distribution for the $E_{cm} = 3.9 - 4.6$ GeV region (all data).

Fig. 6. The $K^0_S\pi^+\pi^-$ mass distribution for $E_{cm} = 4.028$ and 4.415 GeV.

Fig. 7. Comparison of the exotic ($K^{\mp}\pi^{\pm}\pi^{\pm}$) and nonexotic $K^{\mp}\pi^+\pi^-$ mass distributions for the "4.1" GeV region with an M_{recoil} cut 1960 - 2040 MeV/c^2. (a) Exotic, (b) nonexotic.

Fig. 8. (a) M_{recoil} distribution for the $K^{\pm}\pi^{\mp}$ signal as measured. (b) M_{recoil} distribution for the $K^{\pm}\pi^{\mp}$ signal, as well as the kinematic reflection signals "$\pi^+\pi^-$" and "$K\bar{K}$," for fixed nominal $M_{K\pi} = 1865$ MeV/c^2. (c) M_{recoil} distribution for the $K^{\pm}(3\pi)^{\mp}$ signal for fixed $M = 1865$ MeV/c^2. Each distribution is background subtracted as discussed in the text. $E_{cm} = 3.9 - 4.6$ GeV all data.

Fig. 9. M_{recoil} distribution for the $K^{\mp}\pi^{\pm}\pi^{\pm}$ signal for fixed nominal $M_{K\pi\pi} = 1872$ MeV/c^2. The background subtraction comes from the same mass cuts on the nonexotic $K\pi\pi$ channel. $E_{cm} = 3.9 - 4.6$ GeV all data.

Fig. 10. Subtracted recoil spectra for the $K\pi$ and $K\pi\pi$ signals combined. (a) $E_{cm} = 4.028$ GeV. (b) $E_{cm} = 4.415$ GeV.

Fig. 11. (a) $D^0 \to K^-\pi^+$ recoil spectrum at $E_{cm} = 4.028$ GeV computed with a nominal fixed D^0 mass value. (b) $D^0 \to K^-\pi^+$ recoil spectrum at $E_{cm} = 4.41$ GeV. The curves in (a) and (b) show the expected shapes of peaks due to $D\bar{D}^* + \bar{D}D^*$ and $D^*\bar{D}^*$ production at the two E_{cm} values. Here we neglect radiative D^* decays and only show the narrow reflections due to $D^{*0} \to \pi^0 D^0$ decays. In (b) we have also included a third peak centered at 2440 MeV/c^2 with a width $\Gamma = 100$ MeV/c^2.

Fig. 12. Weighted invariant-mass spectrum for $K^{\pm}\pi^{\mp}$ combinations with momenta greater than 1.5 GeV/c at $\langle E_{cm} \rangle = 6.8$ GeV.

Fig. 13. Weighted $D\pi$-D mass difference spectra for (a) $D^0\pi^+$ and $\bar{D}^0\pi^-$ (i.e., $K^{\mp}\pi^{\pm}\pi^{\pm}$) combinations and (b) $\bar{D}^0\pi^+$ and $D^0\pi^-$ (i.e., $K^{\mp}\pi^{\pm}\pi^{\mp}$) combinations. Since there is almost no background below the D^{*+} peak in (a) the probability is high that each event in the peak is real. We gain statistically by replotting with unit weight each event with probability > 0.1. Unweighted $D\pi$-D mass difference spectra for (c) $D^0\pi^+$ and $\bar{D}^0\pi^-$ (i.e., $K^{\mp}\pi^{\pm}\pi^{\pm}$) combinations and (d) $\bar{D}^0\pi^+$ and $D^0\pi^-$ (i.e., $K^{\mp}\pi^{\pm}\pi^{\mp}$) combinations.

Fig. 14. (a) Illustrative example of the contributions to the expected D^0 momentum spectrum near threshold:

$e^+e^- \rightarrow D^{*+}D^{*-}$,	$D^{*+} \rightarrow \pi^+D^0$		(A)
$\rightarrow D^{*0}\bar{D}^{*0}$,	$D^{*0} \rightarrow \pi^0D^0$		(B)
$\rightarrow D^{*0}\bar{D}^{*0}$,	$D^{*0} \rightarrow \gamma D^0$		(C)
$\rightarrow D^{*+}D^-$,	$D^{*+} \rightarrow \pi^+D^0$		(D)
$\rightarrow D^{*0}\bar{D}^0$,	$D^{*0} \rightarrow \pi^0D^0$		(E)
$\rightarrow \bar{D}^{*0}D^0$	direct D^0		(F)
$\rightarrow D^{*0}\bar{D}^0$,	$D^{*0} \rightarrow \gamma D^0$		(G)
$\rightarrow D^0\bar{D}^0$	direct D^0		(H)

(b) $D^0 \rightarrow K^-\pi^+$ momentum spectrum at $E_{cm} = 4.028$ GeV. The solid curve is a typical fit described in text. (c) $D^+ \rightarrow K^-\pi^+\pi^+$ momentum spectrum at $E_{cm} = 4.028$ GeV compared to a typical fit. The dashed curve corresponds to background.

Fig. 15. Dalitz plots, folded around y axis, for the $K\pi\pi$ system with mass cuts $M(K\pi\pi) = 1860 - 1920$ MeV/c^2 and the selections given in Fig. 7. (a) Exotic combination $K^{\mp}\pi^{\pm}\pi^{\pm}$; (b) nonexotic combination $K^{\pm}\pi^+\pi^-$. Here $Q = T_K + T_{\pi_1} + T_{\pi_2}$.

Fig. 16. $M(K^{\mp}\pi^{\pm}\pi^{\pm})$ distribution for the same data sample as in Fig. 15. (a) "Peripheral" and (b) "central" regions (on the folded plot) for a contour of 1^- matrix element as indicated by the shaded regions of the insets; (c) "peripheral" and (d) "central" regions for a contour of a 2^+ matrix element. The solid curves are fits to a Gaussian signal over the scaled backgrounds of Fig. 7b.

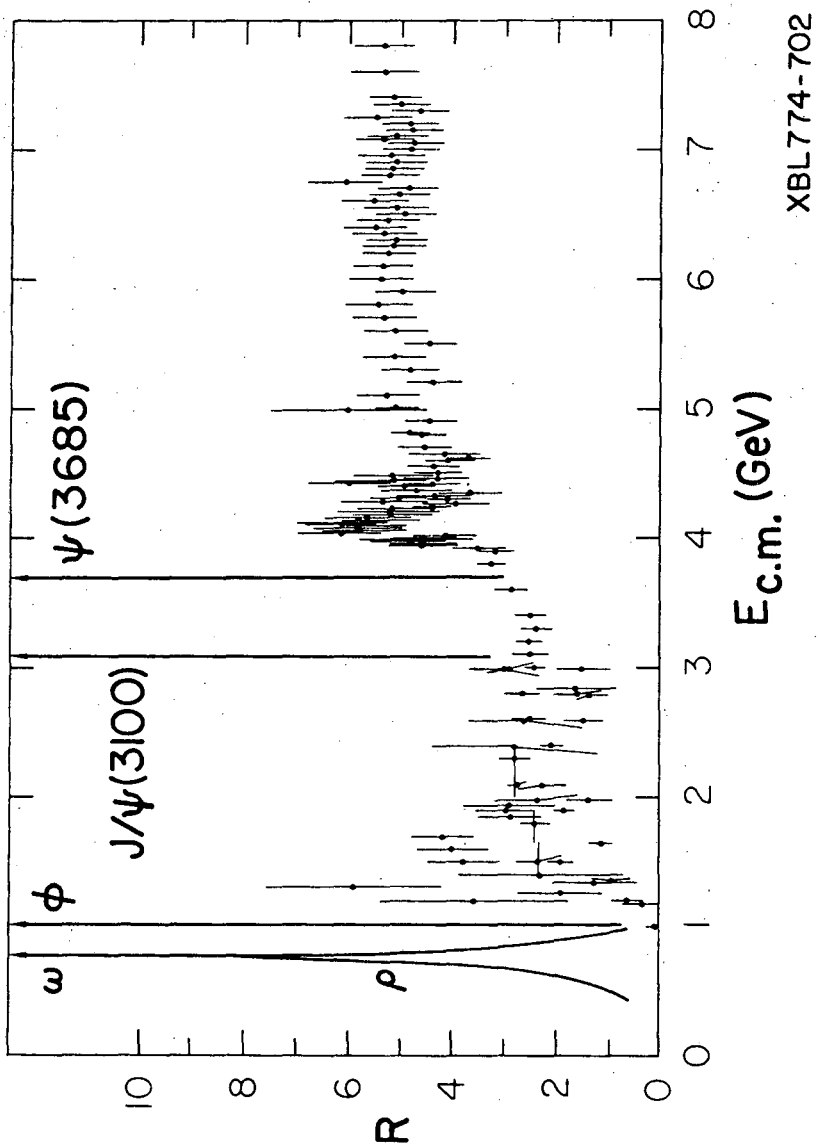

XBL774-702

Fig. 1

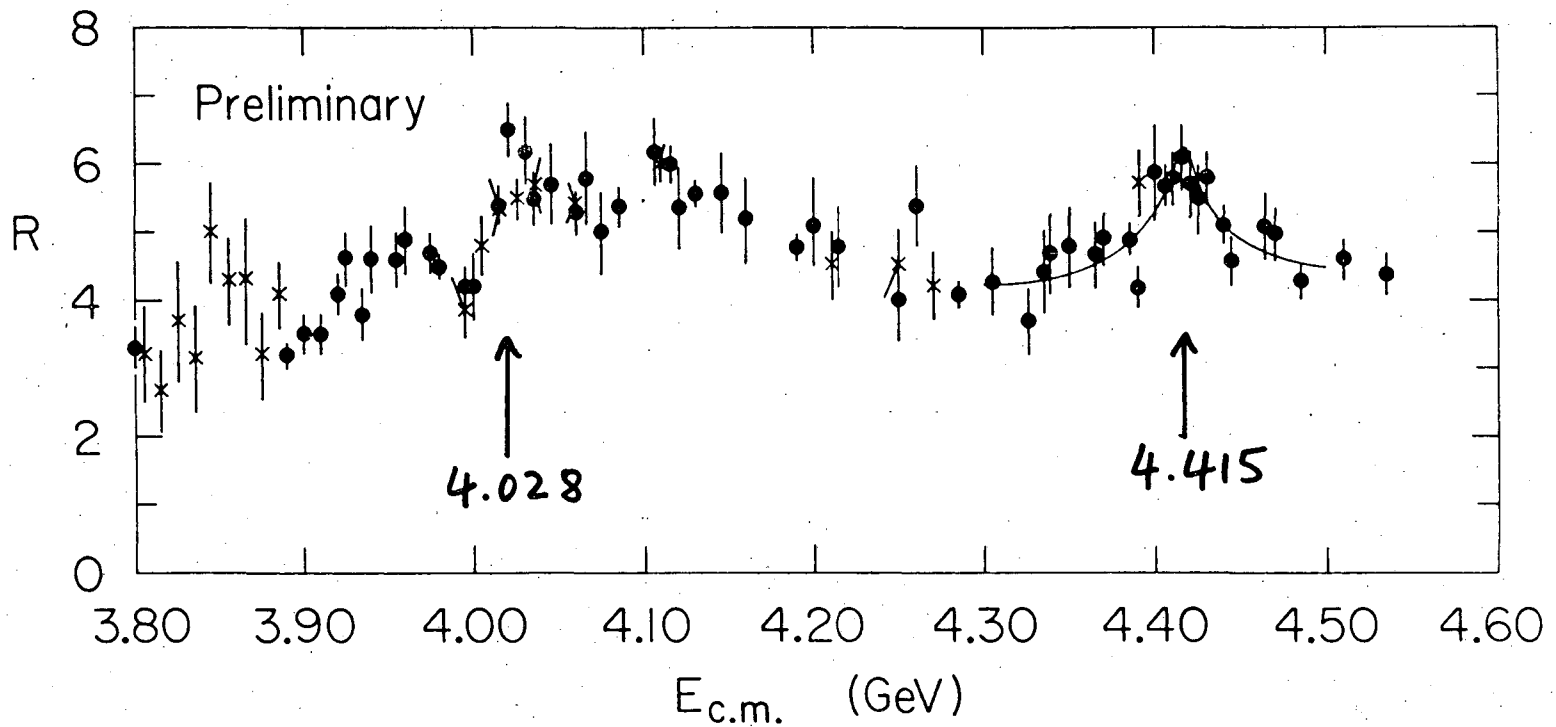

XBL 767-8808

Fig. 2

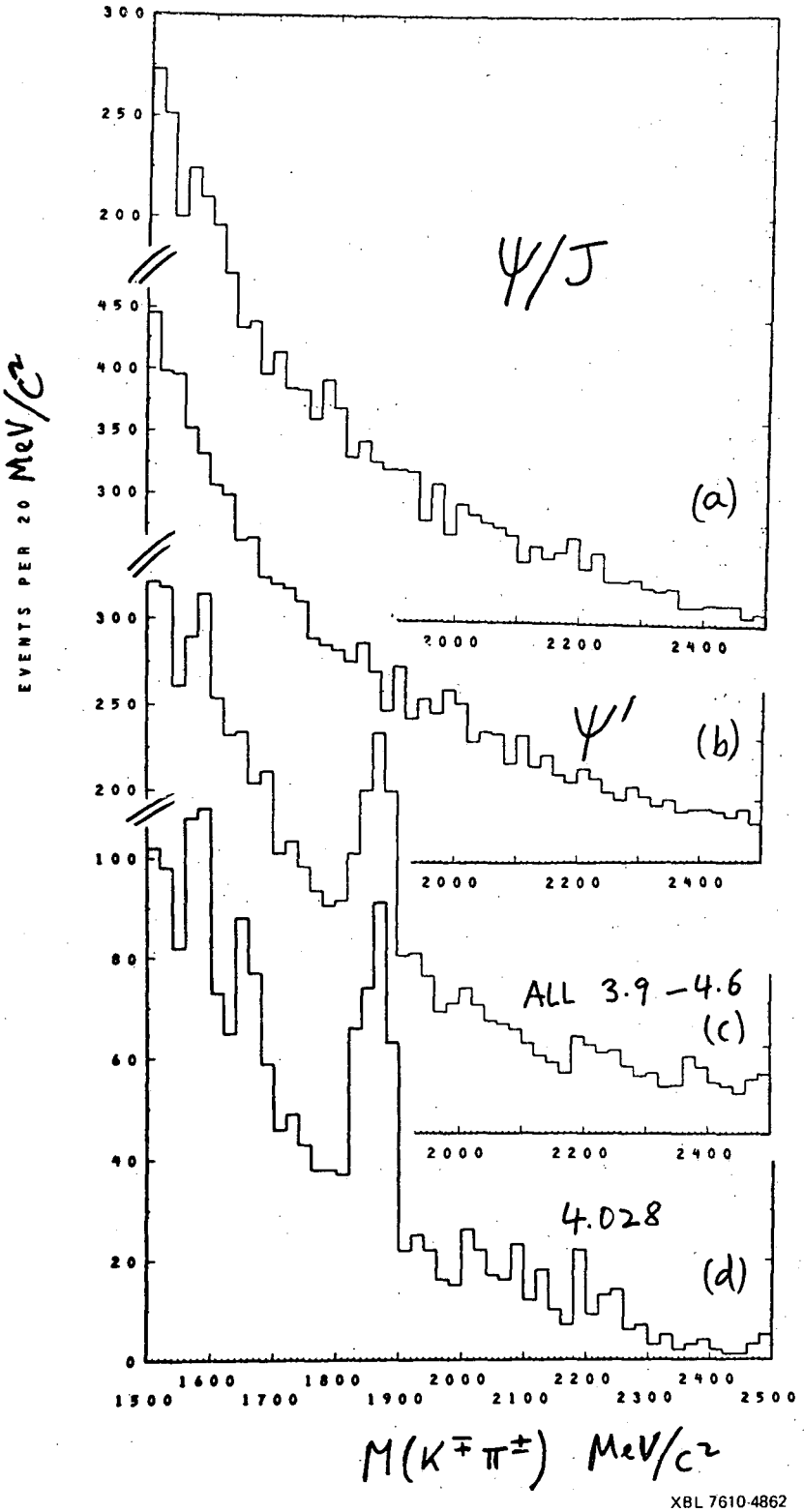
EVENTS PER 20 MeV/c²
ψ/J
(a)
ψ'
(b)
ALL 3.9 – 4.6
(c)
4.028
(d)
M(K∓π±) MeV/c²
XBL 7610-4862

Fig. 3

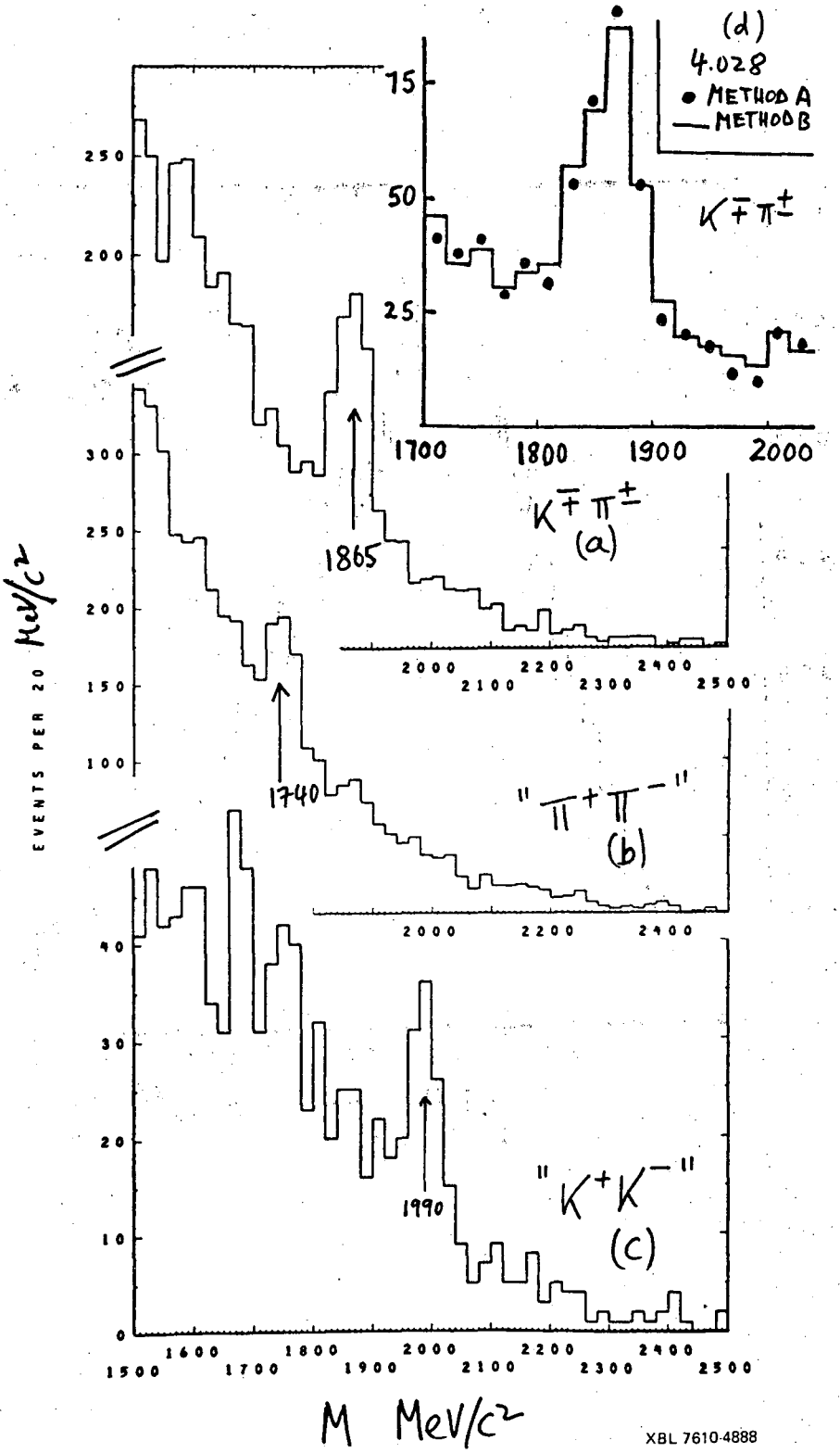

Fig. 4

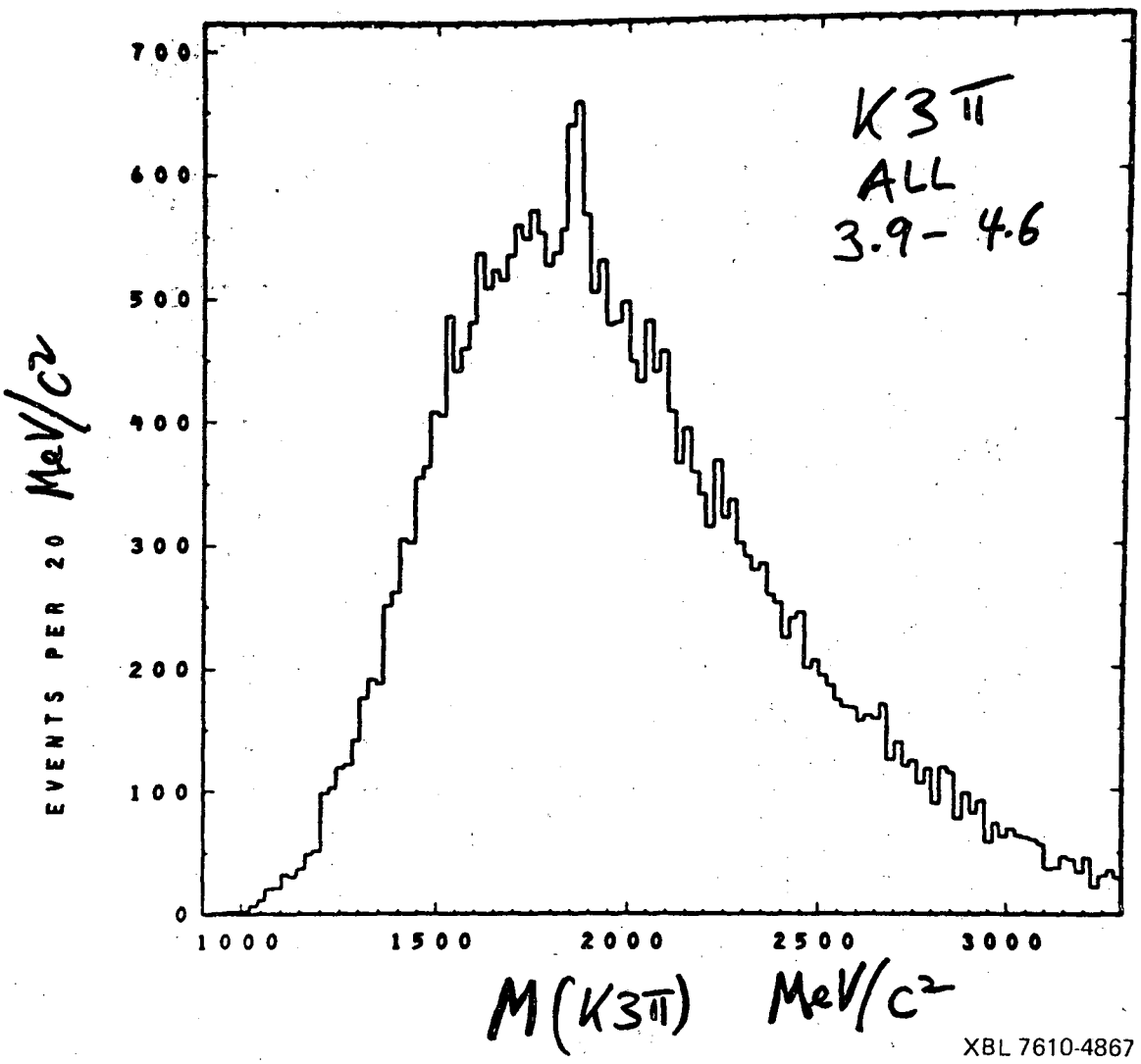
K3π
ALL
3.9 - 4.6
EVENTS PER 20 MeV/c²
0
100
200
300
400
500
600
700
1000
1500
2000
2500
3000
M(K3π) MeV/c²
XBL 7610-4867

Fig. 5

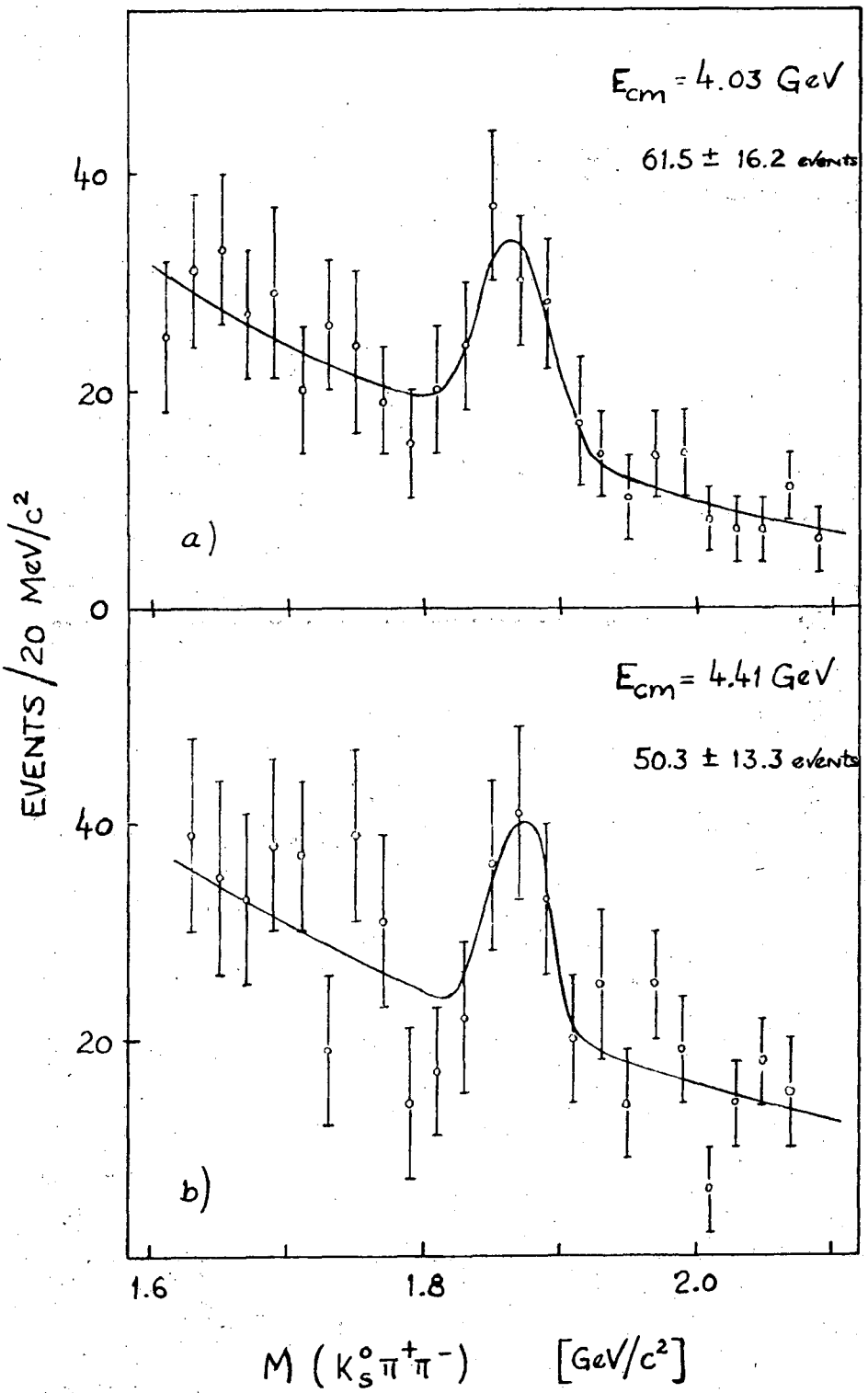

XBL 776-9210

Fig. 6

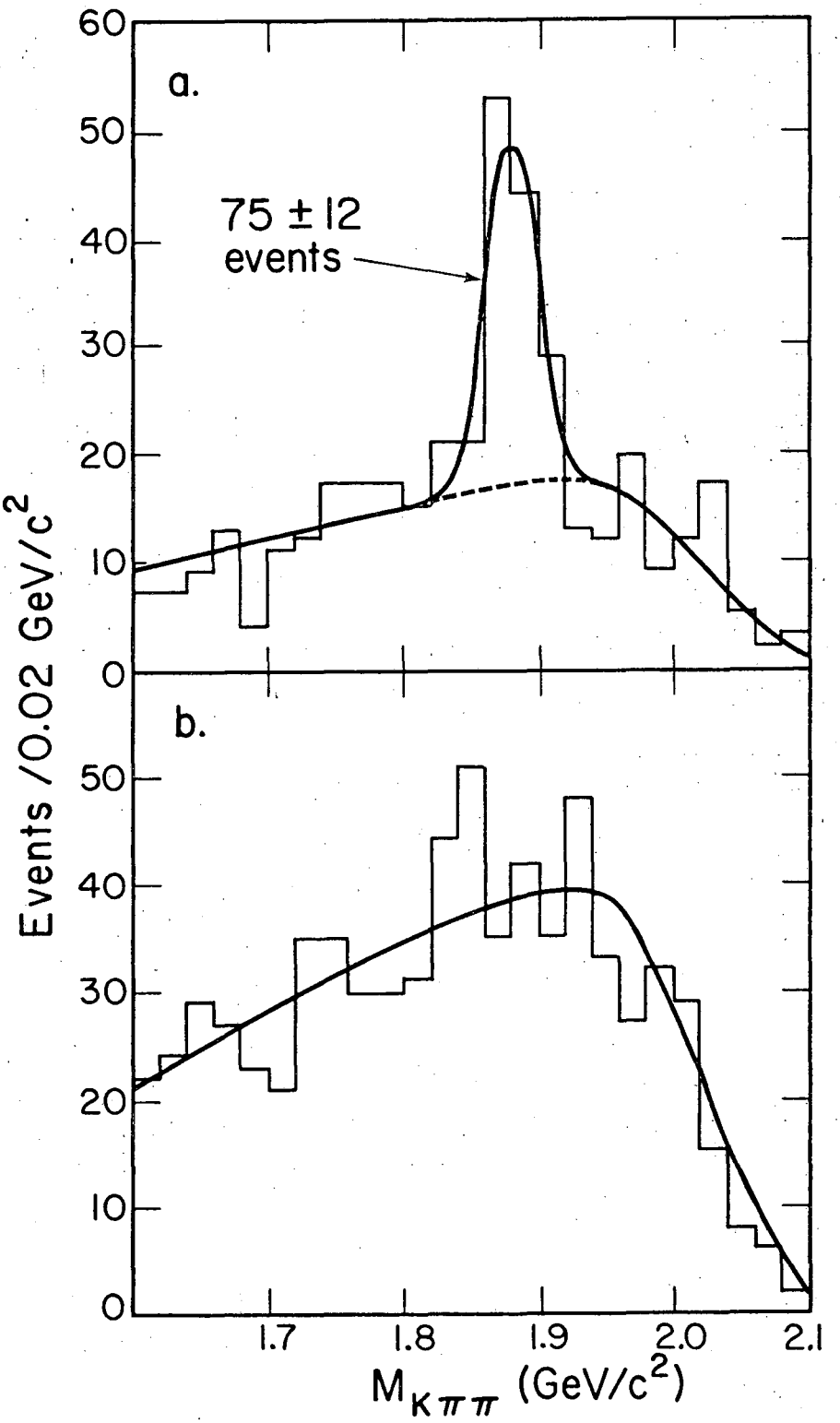

Fig. 7

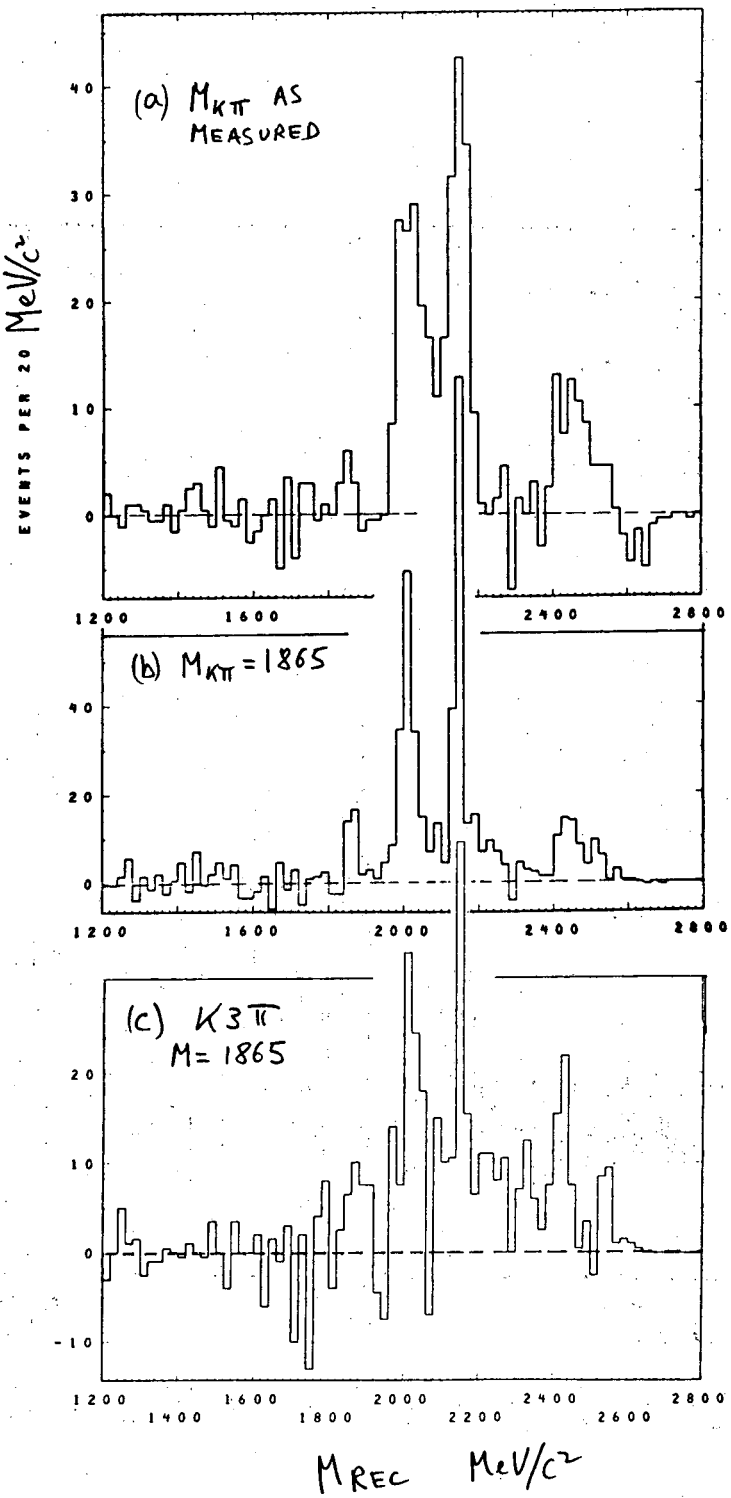

XBL 776-9211

Fig. 8

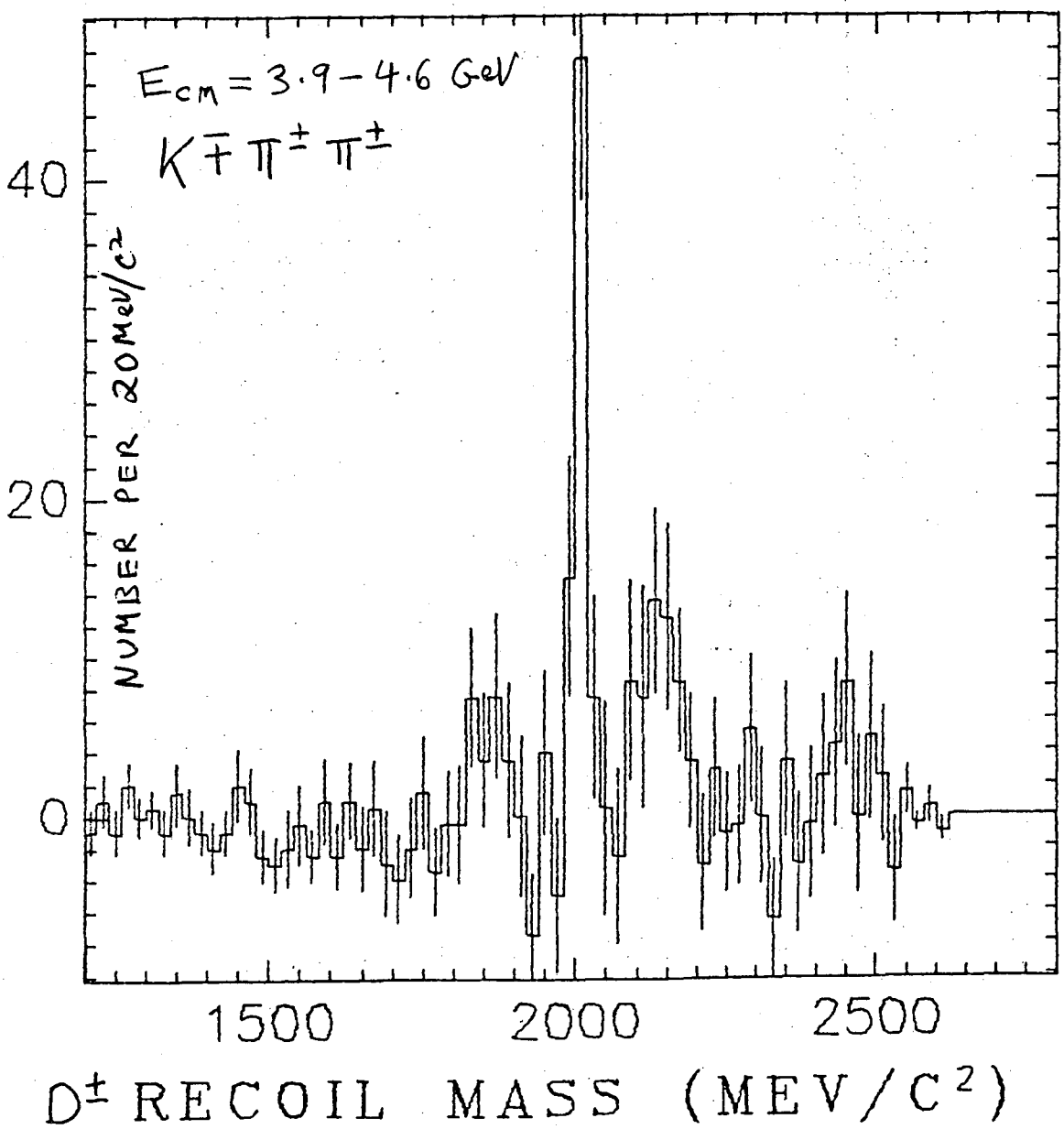
$E_{cm} = 3.9 - 4.6$ GeV
$K\mp\pi^{\pm}\pi^{\pm}$
40
20
0
NUMBER PER 20 MeV/c²
1500
2000
2500
$D^{\pm}$ RECOIL MASS (MEV/C^2)

Fig. 9

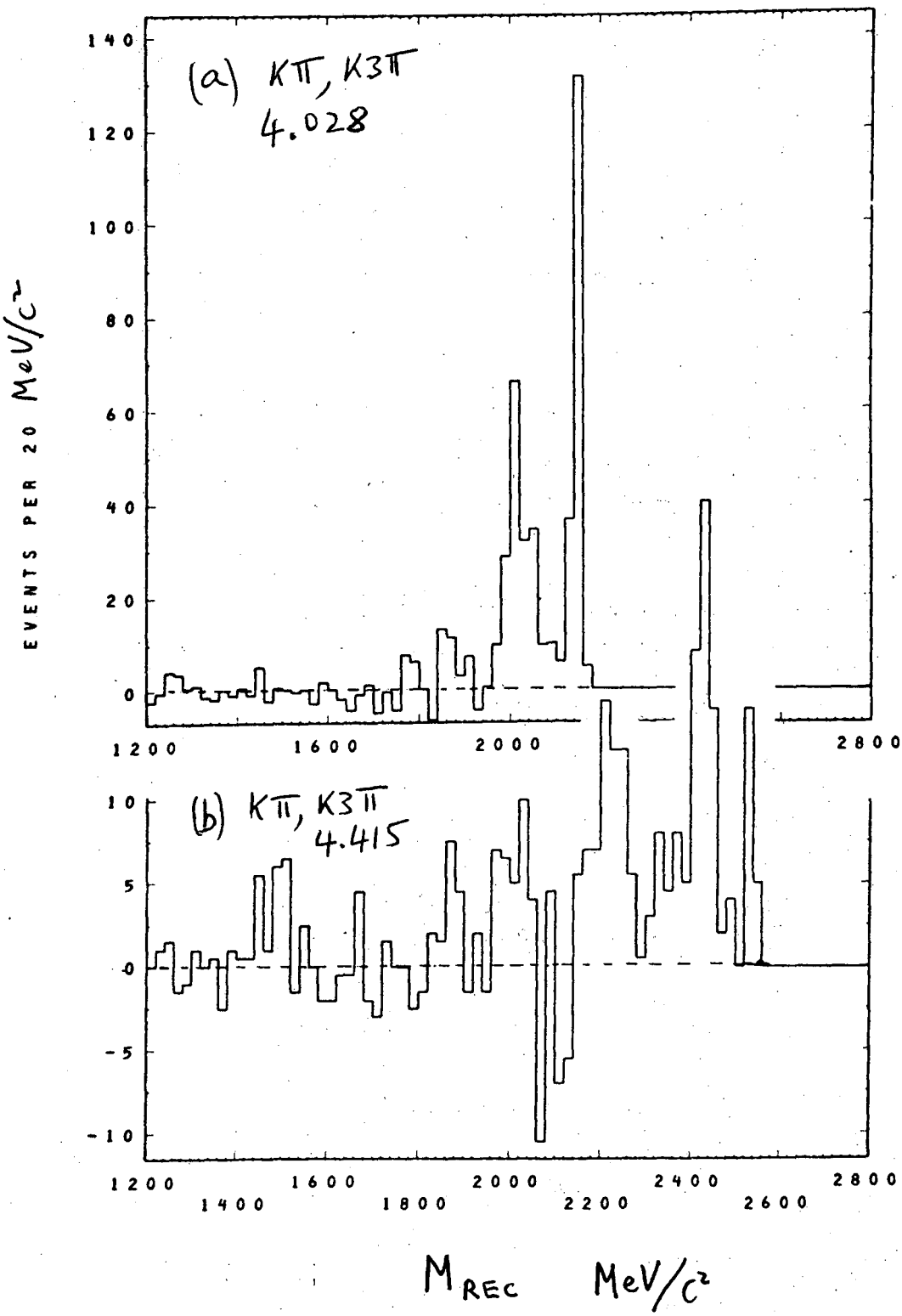

XBL 776-9212

Fig. 10

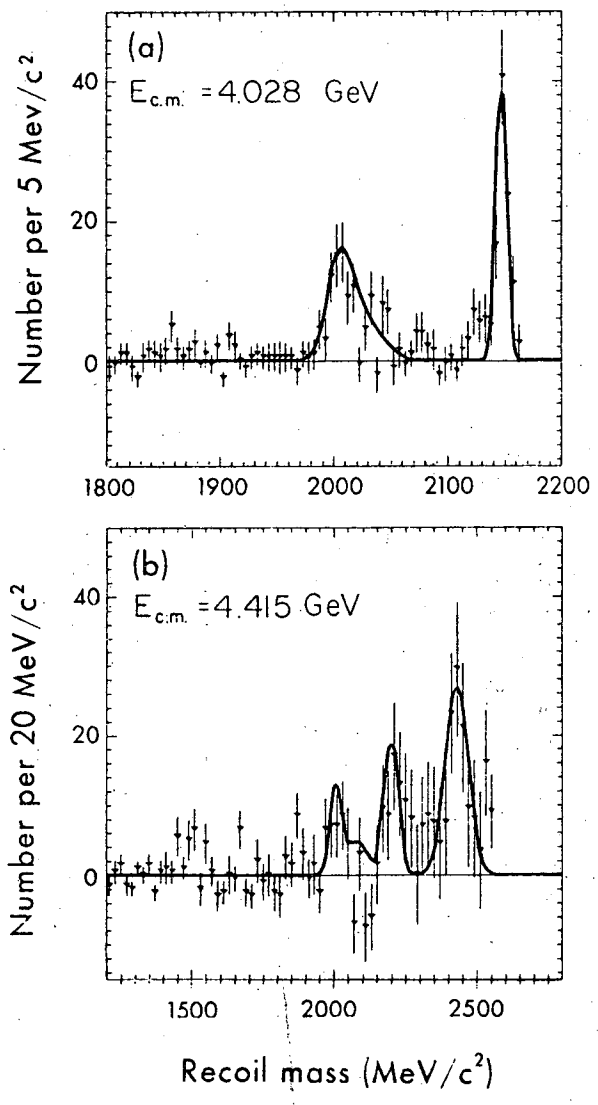
(a)
$E_{c.m.}$ =4.028 GeV
Number per 5 Mev/c²
40
20
0
1800
1900
2000
2100
2200
(b)
$E_{c.m.}$ =4.415 GeV
Number per 20 MeV/c²
40
20
0
1500
2000
2500
Recoil mass (MeV/c²)
XBL776-1170

Fig. 11

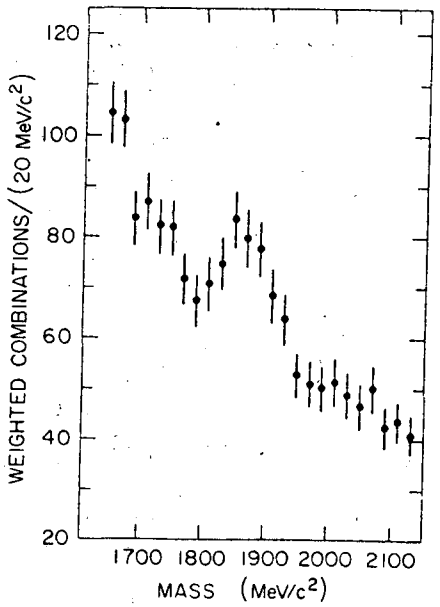

Fig. 12

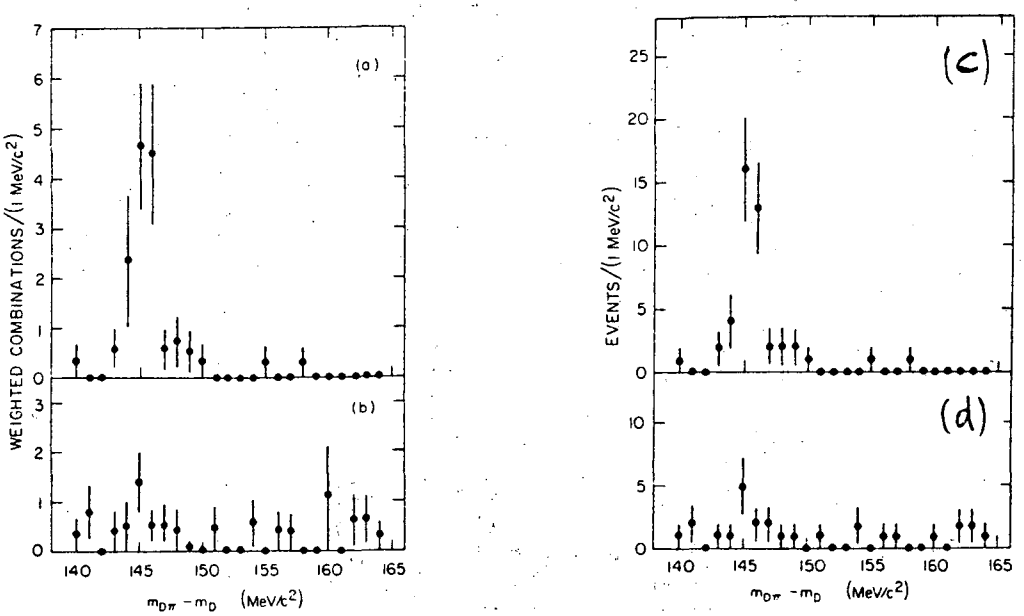

Fig. 13

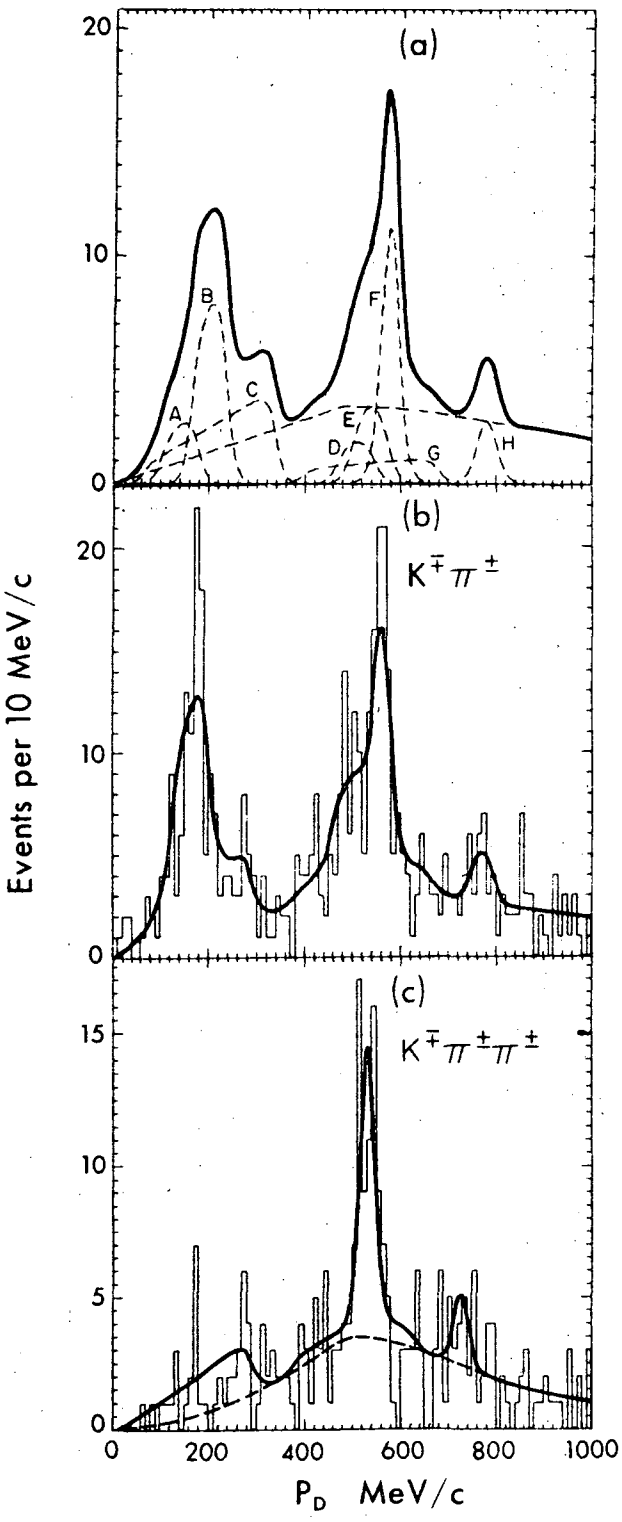

XBL-776-1171

Fig. 14

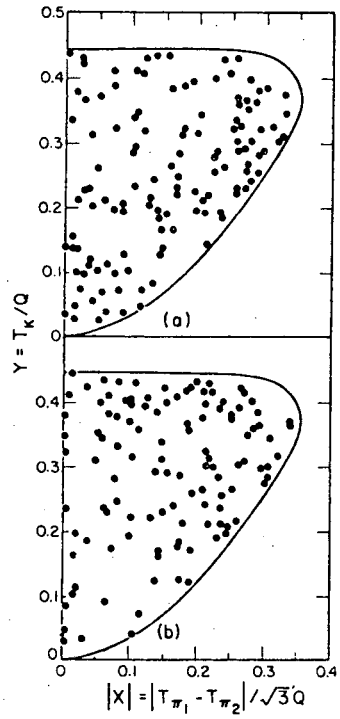
0.5
0.4
0.3
0.2
0.1
0
(a)
(b)
$Y = T_K/Q$
0
0.1
0.2
0.3
0.4
$|X| = |T_{\pi_1} - T_{\pi_2}|/\sqrt{3}Q$

Fig. 15

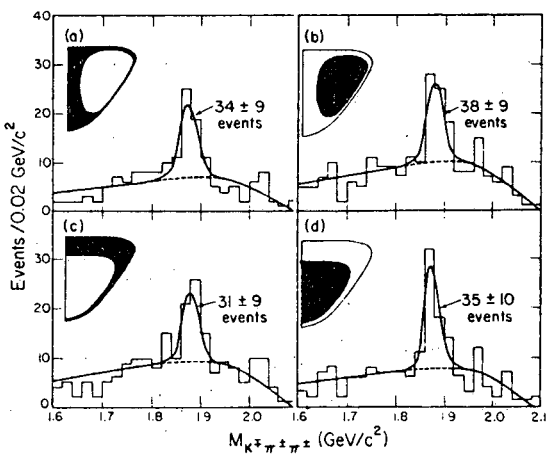
(a)
34 ± 9 events
(b)
38 ± 9 events
(c)
31 ± 9 events
(d)
35 ± 10 events
Events/0.02 GeV/c^2
$M_{K^\pm\pi^\pm\pi^\pm}$ (GeV/c^2)

Fig. 16

TECHNICAL INFORMATION DIVISION
LAWRENCE BERKELEY LABORATORY
UNIVERSITY OF CALIFORNIA
BERKELEY, CALIFORNIA 94720